Resolving hyporheic and groundwater components of streambed water flux using heat as a tracer

Aditi S. Bhaskar,[1,2] Judson W. Harvey,[2] and Eric J. Henry[3]

Received 21 December 2011; revised 19 June 2012; accepted 26 June 2012; published 29 August 2012.

[1] Hyporheic and groundwater fluxes typically occur together in permeable sediments beneath flowing stream water. However, streambed water fluxes quantified using the thermal method are usually interpreted as representing either groundwater or hyporheic fluxes. Our purpose was to improve understanding of co-occurring groundwater and hyporheic fluxes using streambed temperature measurements and analysis of one-dimensional heat transport in shallow streambeds. First, we examined how changes in hyporheic and groundwater fluxes affect their relative magnitudes by reevaluating previously published simulations. These indicated that flux magnitudes are largely independent until a threshold is crossed, past which hyporheic fluxes are diminished by much larger (1000-fold) groundwater fluxes. We tested accurate quantification of co-occurring fluxes using one-dimensional approaches that are appropriate for analyzing streambed temperature data collected at field sites. The thermal analytical method, which uses an analytical solution to the one-dimensional heat transport equation, was used to analyze results from a numerical heat transport model, in which hyporheic flow was represented as increased thermal dispersion at shallow depths. We found that co-occurring groundwater and hyporheic fluxes can be quantified in streambeds, although not always accurately. For example, using a temperature time series collected in a sandy streambed, we found that hyporheic and groundwater flow could both be detected when thermal dispersion due to hyporheic flow was significant compared to thermal conduction. We provide guidance for when thermal data can be used to quantify both hyporheic and groundwater fluxes, and we show that neglecting thermal dispersion may affect accuracy and interpretation of estimated streambed water fluxes.

Citation: Bhaskar, A. S., J. W. Harvey, and E. J. Henry (2012), Resolving hyporheic and groundwater components of streambed water flux using heat as a tracer, *Water Resour. Res.*, *48*, W08524, doi:10.1029/2011WR011784.

1. Introduction

[2] Movement of stream water across the bed and banks of streams into shallow subsurface flow paths that return to the stream defines hyporheic flow, a ubiquitous component of groundwater-surface water interactions [*Winter et al.*, 1998]. Although hyporheic flow paths are small in scale, they often conduct substantial water fluxes relative to the larger-scale groundwater flow systems within which they are embedded [*Stonedahl et al.*, 2010]. The need to distinguish between groundwater and hyporheic components of groundwater-surface water interactions arises from the desire of many researchers to characterize the biogeochemical conditions and ecological processes of each flow type [*Jones and Mulholland*, 2000]. Hyporheic flow paths can have different temperatures and chemical conditions than groundwater discharge flow paths located in close proximity [*Arrigoni et al.*, 2008; *Fanelli and Lautz*, 2008]. Researchers have also demonstrated numerous important biologically mediated processes occurring in hyporheic zones, including enhanced removal of metal and nutrient contaminants from flowing stream water [*Böhlke et al.*, 2009; *Fuller and Harvey*, 2000; *Triska et al.*, 1989; *Valett et al.*, 1996], enhanced respiration of organic carbon [*Haggerty et al.*, 2009], modulation of stream temperatures [*Arrigoni et al.*, 2008; *Gerecht et al.*, 2011], and effects of land use change and stream restoration on these processes [*Groffman et al.*, 2005; *Kaushal et al.*, 2008].

[3] Streambed water temperatures also have direct relevance to biogeochemical reaction rates, ecological processes, and fish health [*Caissie*, 2006; *Nelson and Palmer*, 2007; *Wang and Kanehl*, 2003]. Because of the effects on ecological processes, there is interest in the impacts of land use change and climate change on stream temperatures [*Kaushal et al.*, 2010]. In urbanized areas, stream temperatures can increase significantly due to reduced riparian vegetation coverage [*Beschta*, 1997; *Poole and Berman*, 2001], runoff

[1]Center for Urban Environmental Research and Education, Department of Chemical, Biochemical, and Environmental Engineering, University of Maryland, Baltimore County, Baltimore, Maryland, USA.
[2]U.S. Geological Survey, Reston, Virginia, USA.
[3]Department of Geography and Geology, University of North Carolina at Wilmington, Wilmington, North Carolina, USA.

Corresponding author: A. S. Bhaskar, Center for Urban Environmental Research and Education, Department of Chemical, Biochemical, and Environmental Engineering, University of Maryland, Baltimore County, 1000 Hilltop Circle, TRC Room 105, Baltimore, MD 21250, USA. (aditi.bhaskar@umbc.edu)

0043-1397/12/2011WR011784

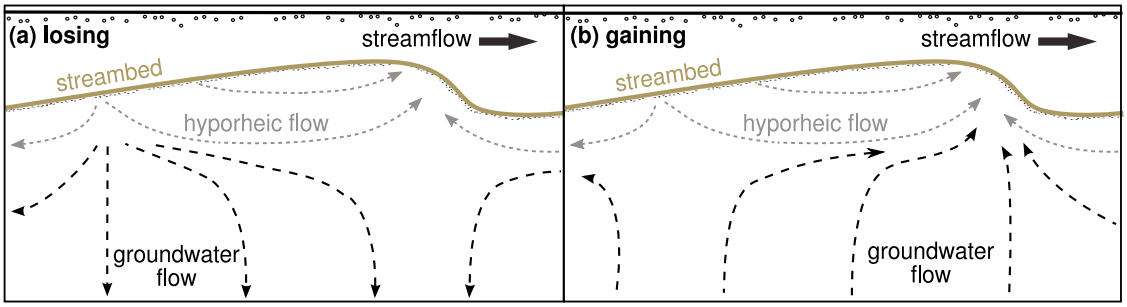

Figure 1. Conceptual diagrams illustrate hyporheic flow interacting with groundwater flow beneath bed forms. Hyporheic flow co-occurring (a) with recharge in a losing stream and (b) with groundwater discharge in a gaining stream are shown.

from hot impervious surfaces [*Galli*, 1990], warm wastewater inputs [*Kinouchi et al.*, 2007], and changes in stream hydraulic geometry [*LeBlanc et al.*, 1997]. A greater understanding of the interactions between hyporheic and groundwater fluxes is needed in order to predict how hydraulics, stream ecology, and biogeochemistry will coevolve in response to changing land use.

[4] Hyporheic exchange fluxes can be driven by an uneven streambed pressure distribution created by streamflow over roughness features such as ripples, dunes, sandbars, and meander bends, which leads to nesting of hyporheic flow paths at many different scales [*Elliott and Brooks*, 1997a; *Harvey and Bencala*, 1993]. Small-scale (centimeters to meters) hyporheic flow paths beneath and to the side of streams typically are embedded within larger-scale (meters to tens of meters) pathways of groundwater discharge and recharge [*Stonedahl et al.*, 2010]. Hyporheic exchange fluxes also are responsive to hydraulic gradient-driven forces, both near and far from the stream, and therefore share a common pressure distribution and are intimately connected with groundwater fluxes. Due to the shared pressure distribution, hyporheic exchange fluxes can be suppressed by groundwater discharge (upward groundwater flow to a gaining stream) [*Harvey et al.*, 1996; *Wondzell and Swanson*, 1996] or groundwater recharge (downward groundwater flow from a losing stream) [*Cardenas and Wilson*, 2007]. As shown in numerical modeling [*Boano et al.*, 2008, 2009; *Cardenas and Wilson*, 2007], groundwater discharge counters the downwelling part of hyporheic flow paths and decreases the area over which stream water enters hyporheic flow paths. Conversely, groundwater recharge counters the upwelling part of hyporheic flow paths and decreases the area over which stream water exits hyporheic flow paths [*Cardenas and Wilson*, 2007]. In both cases, increased groundwater flow leads to reduced hyporheic exchange depth and overall hyporheic flow.

[5] Hydraulic data and data from in-stream solute tracer experiments have both been used to partition groundwater and hyporheic contributions to total surface-subsurface exchange [*Bianchin et al.*, 2010; *Harvey et al.*, 1996; *Hester and Doyle*, 2008; *Storey et al.*, 2003; *Wondzell and Swanson*, 1996; *Wroblicky et al.*, 1998]. Stream tracer experiments have the advantage of spatial averaging at the reach scale, but "exchange" measurements cannot be uniquely ascribed to hyporheic exchange unless supported by detailed subsurface measurements [e.g., *Harvey and Fuller*, 1998; *Triska et al.*, 1989]. Tracer-based approaches also are difficult to implement during periods of changing flow. Hydraulic-based approaches are better suited for quantifying changing proportions of hyporheic and groundwater fluxes and comparing them between times of low and high streamflow [e.g., *Harvey et al.*, 1996, Table 1]. Those methods, however, are subject to significant error associated with hydraulic conductivity estimation. Both hydraulic and tracer-based measurements are expensive and time consuming—even for periods of steady flow.

[6] Using heat as a tracer of co-occurring hyporheic and groundwater fluxes is attractive due to its low cost and the opportunity to collect high temporal resolution data sets for determining how fluxes change with time [*Stonestrom and Constantz*, 2003]. Heat tracing typically has only been used to quantify unidirectional fluxes across the streambed, which have been ascribed to groundwater recharge or discharge fluxes [*Conant*, 2004; *Constantz et al.*, 2003; *Silliman et al.*, 1995]. More recently, temperature tracing has been applied to quantify streambed exchange due to relatively large (i.e., meter-scale) "hyporheic" flow paths [*Fanelli and Lautz*, 2008; *Gerecht et al.*, 2011; *Hester et al.*, 2009; *Swanson and Cardenas*, 2010]. *Bianchin et al.* [2010] modeled streambed temperature as part of their larger study on groundwater-surface water interactions but did not partition hyporheic and groundwater fluxes using temperature data. Whereas the use of heat as a tracer in streambeds has been widely applied for determining either groundwater or hyporheic fluxes across streambeds, it has not, to our knowledge, been tested for simultaneously quantifying both hyporheic and groundwater components of the total streambed flux.

[7] The physical characteristics of mixing and transport at the interface between hyporheic and groundwater flow has been investigated from a theoretical perspective [*Boano et al.*, 2008, 2009; *Cardenas and Wilson*, 2007]. *Elliott and Brooks* [1997a, 1997b] demonstrated the utility of a one-dimensional approximation of three-dimensional hyporheic flow as a vertical diffusive-like flux (see section 2.3). In the present work, we build on these studies by testing whether analysis of streambed temperatures with thermal modeling methods can quantify both bed form-driven hyporheic and groundwater flow, such as those shown in Figure 1. We reexamine the modeling results of *Cardenas and Wilson* [2007] to determine the ranges of interdependence of hyporheic and groundwater flow. We then conduct numerical experiments using VS2DH to study the detection of each flux type using the analytical method of *Hatch et al.* [2006].

Last, we apply our approach to analyze flux components during base flow and a flood in a sand-bed stream of North Carolina.

2. Theory

2.1. One-Dimensional Heat Transport in Streambeds

[8] Heat is transmitted through the streambed by advection and hydrodynamic dispersion in flowing water and by heat conduction through streambed sediments. These terms are represented by the vertical one-dimensional heat transport equation

$$\frac{\partial T}{\partial t} = \kappa_e \frac{\partial^2 T}{\partial z^2} - q_{gw} \frac{C_w}{C} \frac{\partial T}{\partial z} \quad (1)$$

where T is temperature, κ_e is effective thermal diffusivity, C_w is heat capacity of the fluid, C is heat capacity of the sediment fluid mix, q_{gw} is the vertical flux of groundwater per unit area, z is depth, and t is time. Symbol definitions and associated units are summarized in the notation section. By convention, positive advective fluxes ($q > 0$) indicate downward flow into the streambed (representing a losing stream and groundwater recharge), and negative fluxes ($q < 0$) indicate upward flow from the streambed to surface water (a gaining stream and groundwater discharge). The thermal diffusivity term κ_e represents the summation of heat conduction and hydrodynamic dispersion: $\kappa_e = \frac{\lambda}{C} + D_T$, where λ is thermal conductivity and D_T is hydrodynamic dispersion of heat.

[9] Thermal conduction, which occurs through sediment and water, is efficient relative to the analogous process of solute diffusion, which only occurs through water [*Molina-Giraldo et al.*, 2011]. Because of its efficiency, thermal conduction is often considered to be the dominant term in thermal diffusivity compared with hydrodynamic dispersion in groundwater transport [*Anderson*, 2005; *Ingebritsen et al.*, 2006; *Keery et al.*, 2007; *Rau et al.*, 2010; *Swanson and Cardenas*, 2010]. We found that hydrodynamic dispersion of heat cannot always be ignored in the hyporheic zone and may, in fact, provide a signal that is useful to characterize hyporheic flow.

2.2. Hydrodynamic Dispersion of Heat

[10] The thermal Peclet number is the ratio of advective to conductive heat flux [*Anderson*, 2005]. For example, using an example mean grain diameter as the representative length (3.8×10^{-4} m) and combining it with an example vertical groundwater flux (1×10^{-6} m/s) gives a thermal Peclet number of 7×10^{-4}. This value falls within a range where heat conduction dominates over heat advection. Whether thermal dispersion depends linearly on fluid velocity, as solute dispersion does, is currently a subject of debate [*Anderson*, 2005; *Molina-Giraldo et al.*, 2011]. A linear dependence implies that thermal dispersion can be expressed as the product of the velocity and a parameter known as the thermal dispersivity [*Anderson*, 2005]. *Metzger et al.* [2004] and *Rau et al.* [2012] experimentally found that the longitudinal thermal dispersion coefficient scales nonlinearly with the thermal Peclet number at low Peclet numbers.

[11] For the small thermal Peclet number in our groundwater system, dispersivity calculated using the nonlinear relationship of *Molina-Giraldo et al.* [2011, equation (20)] is on the order of 10^{-7} m, which is within a range where dispersion is negligible compared to conduction [*Molina-Giraldo et al.*, 2011; *Rau et al.*, 2012]. At larger thermal Peclet numbers typical of bed form-scale hyporheic flow at our site, thermal dispersion is approximately linearly related to Peclet number. Therefore, for large values of the thermal Peclet number, it appears that the contribution of heat conduction is minimal and that the hydrodynamic dispersion of heat can be assumed to be analogous to dispersion of a conservatively transported solute tracer in water. These observations support our use of thermal dispersion modeling for quantifying hyporheic flow.

2.3. Extending the One-Dimensional Analysis to Quantify Both Hyporheic and Groundwater Fluxes

[12] In this paper, we consider whether hyporheic flow will enhance vertical thermal dispersion enough to allow both hyporheic and groundwater flow to be simultaneously estimated from analysis of heat transport using equation (1). Our approach follows directly from previous research [e.g., *Elliott and Brooks*, 1997b, 1997b; *O'Connor and Harvey*, 2008; *Packman and Salehin*, 2003; *Richardson and Parr*, 1988] where one-dimensional modeling of effective diffusion was used to simulate fluxes caused by three-dimensional hyporheic flow paths. For example, *Elliott and Brooks* [1997a and 1997b] demonstrated that measurements of bed form-scale hyporheic flow in a flume could be modeled by two-dimensional simulation of hyporheic flow that, importantly, can be further reduced to a one-dimensional (vertical) analysis of diffusive-like exchange with the streambed. Several researchers have gone on to use the effective diffusion modeling approach to quantify hyporheic transport and relate it to measurable physical variables, such as hydraulic forces that drive hyporheic flow and the sediment properties that resist hyporheic flow [e.g., *O'Connor and Harvey*, 2008; *Packman and Salehin*, 2003; *Richardson and Parr*, 1988].

[13] We conceptualize subsurface flow as occurring in a layered system with hyporheic and groundwater flow co-occurring in the shallow streambed (centimeters below the stream) where heat transport is dominated by vertical hydrodynamic dispersion, above a lower layer where heat transport is dominated by vertical groundwater advection. Application of the steady state, one-dimensional, advection-conduction heat equation requires that the advective flux be constant with depth to preserve continuity of water flow. Thus we associate the advective flux term only with the vertical flux of groundwater and quantify hyporheic flow as a vertical dispersive flux of heat. The resulting effective dispersion coefficient can easily be evaluated in terms of a water exchange flux using a well-known relation between effective diffusion and mass transfer into a layered medium (discussed in section 3.2.1). A one-dimensional approximation of hyporheic flow is most relevant when hyporheic flow paths are small (e.g., centimeter-scale bed form-driven hyporheic flow) relative to the depth of emplacement of temperature sensors, the depth of the model domain, and the scale of groundwater flow paths (typically meter scale or larger). Larger-scale hyporheic flow (greater than tens of centimeters) below bars, large wood debris, restoration structures, etc., will be difficult to account for as a dispersive flux unless the features are closely spaced and the domain of interest increases accordingly.

[14] Whether heat transport by hyporheic flow can be detected as a thermal dispersive flux depends on whether thermal hydrodynamic dispersion dominates conduction in the thermal diffusivity term [*Green et al.*, 1964]. The dimensionless ratio of thermal dispersion to thermal conduction $\left(\frac{D_T}{\frac{\lambda}{C}}\right)$, the thermal diffusivity index, can be a useful guide. When this ratio is less than 0.1, only heat conduction is an important contributor to thermal diffusivity, which is what has typically been assumed for groundwater. If the dispersive transport signal caused by hyporheic flow is comparable to or larger than transport caused by heat conduction (e.g., if the ratio is between 0.5 and 3), then hydrodynamic dispersion of heat is significant. If the ratio is greater than 3, then hydrodynamic dispersion of heat dominates heat conduction as a transport mechanism. If dispersion is significant or dominant relative to conduction, the thermal diffusivity parameter of equation (1) can be used as a fitting parameter to quantify hyporheic transport, which leaves the advection term q_{gw} to be fitted to temperatures in the lower part of the streambed to quantify groundwater flux.

3. Methods

3.1. Analytical and Numerical Simulations With Hyporheic and Groundwater Flow

3.1.1. Thermal Analytical Methods to Determine Streambed Fluxes

[15] *Hatch et al.* [2006] and *Keery et al.* [2007] developed analytical methods that are now commonly used to determine vertical streambed fluxes from pairs of temperature sensors at different depths in streambed sediments, based on earlier work [*Goto et al.*, 2005; *Stallman*, 1965; *Suzuki*, 1960]. Our work quantifies the magnitude and direction of vertical fluxes using the ratio between diel peak-to-peak amplitudes of temperature measurements at two depths in the streambed [*Hatch et al.*, 2006]. This relationship was used because it was previously found to be more accurate under most conditions than the time lag relationship also presented in *Hatch et al.* [2006] and can also provide flux directionality [*Lautz*, 2010]. Equation (6a) in *Hatch et al.* [2006] gives the thermal front velocity $v\left(=\frac{C_w}{C}q_{gw}\right)$ that is used to calculate vertical fluid flux:

$$v = \frac{2\kappa_e}{\Delta z}\ln A_r + \sqrt{\frac{\alpha+v^2}{2}} \tag{2}$$

where Δz is distance between temperature sensors, A_r is amplitude ratio, $\alpha = \sqrt{v^4 + \left(\frac{8\pi\kappa_e}{P}\right)^2}$, and P is period of temperature variation. The amplitude ratio was calculated for each temperature observation point (either modeled or from field data) using the adjacent sensor as its pair, where adjacent indicates the closest, shallower measurement on the same temperature ladder.

[16] Application of the analytical solution assumes (a) one-dimensional flow in which fluid velocity is steady and uniform along the z axis, (b) heat properties of the fluid and porous media are constant in space and time, (c) water temperature equals that of the surrounding sediment, (d) surface water temperature has a sinusoidal form with constant amplitude, (e) temperature at infinite depth is constant, and (f) there is no thermal gradient with depth. *Shanafield et al.* [2011] analyzed the uncertainty in input parameters to the thermal analytical method and found accuracy in sensor spacing and temperature variations were most important for accurate flux estimates. *Lautz* [2010] tested the effects of violations of some of the assumptions of the method and found the violation of the one-dimensional flow assumption to cause some of the largest errors. In a field setting, hyporheic exchange and its interactions with groundwater flow could be one reason for violation of the assumption of constant vertical flux, which potentially can be addressed through representing hyporheic flux as enhanced thermal dispersion. We began by testing the thermal analytical method by analyzing temperature time series generated by a numerical model. We then applied both the thermal analytical method and the numerical model to analyze temperature time series collected at a field site.

3.1.2. Thermal Numerical Simulations for Testing the Analytical Model

[17] VS2DH [*Healy and Ronan*, 1996] is a numerical model that solves the heat transport equation in two-dimensional variably saturated porous media using a finite difference approximation. Using VS2DH, and the graphical user interface VS2DI [*Hsieh et al.*, 2000], we performed one-dimensional numerical experiments which include ambient groundwater flow and use the enhanced thermal dispersion approach to incorporate hyporheic fluxes in a variety of scenarios. The simulated temperature series at various depths were then analyzed using the thermal analytical method of *Hatch et al.* [2006] to determine vertical flux. The flux calculated with the analytical method was compared to the originally specified groundwater and hyporheic fluxes. Parameters used for these and later field site simulations (discussed in section 3.2) are given in Table 1.

[18] The domain used for numerical experiments was designed to best approximate the assumptions of the analytical method of *Hatch et al.* [2006]. The one-dimensional domain was 1 m deep, which sufficiently approximated an infinitely deep domain. The surface boundary condition was constant hydraulic head of 0 m and had a sinusoidally varying daily temperature with a constant amplitude of 1°C. The bottom boundary condition was constant hydraulic head of ±0.01 m (positive for upward groundwater flow) and temperature equal to the mean surface water temperature of 20°C. Both lateral boundary conditions were no fluid and temperature flux and, along with a one-cell-wide domain, allowed for a one-dimensional simulation. The initial conditions were set to agree with the flux and temperature specified at the boundaries early in the simulation. Observation points, depths at which output was generated, were located every 1 cm for the top 10 cm and every 5 cm for depths between 10 and 50 cm. The simulation was run for 10 days with 5 min time steps. To minimize the effects of initial conditions, the last day of simulation was analyzed. All parameters used were constant throughout the domain, except for dispersion, which was used to vary hyporheic flux.

[19] Within the numerical model VS2DH, thermal dispersion is defined as $D_T = \beta\frac{q_{gw}}{\theta}$, where $\frac{q_{gw}}{\theta}$ is linear fluid velocity, θ is porosity, and β is thermal dispersivity [*Healy and Ronan*, 1996]. Therefore, we implemented enhanced thermal dispersion within the hyporheic zone in VS2DH

Table 1. Thermal Parameters Used for VS2DH Modeling and Thermal Analytical Analysis and Their Sources[a]

Parameter	Value	Units	Source
Total porosity (θ)	0.4		Field measurement
Average dry bulk density	1.60	g/cm^3	Field measurement
Thermal conductivity (λ)	2.3012	J/s-m-°C	Figure 2 in *Lapham* [1989]
Heat capacity of sediment-water mix (C)	2,641,150	J/m^3-°C	Figure 2 in *Lapham* [1989]
Heat capacity of water (C_w)	4,181,800	J/m^3-°C	At 20°C
Hydraulic conductivity (K)	1×10^{-4}	m/s	Picked for numerical experiments
	3.3×10^{-4}	m/s	Field measurement
Period of temperature signal (P)	86400	s	Picked to analyze diurnal signals
Thermal diffusivity (κ_e)	8.7×10^{-7}	m^2/s	Calculation, λ/C
Specific storage (S_s)	0	1/m	Picked for numerical experiments
	1×10^{-4}	1/m	*Bredehoeft and Hanshaw* [1968]
Heat capacity of dry sediment (C_s)	1,614,050	J/m^3-°C	Calculation using volume sediment and water fractions

[a]Values of hydraulic conductivity and specific storage were picked for simplicity in the numerical experiments and are different than the values used for the simulation of field measurements.

simulations by varying thermal dispersivity. The linear vertical velocity as modeled by VS2DH is equal to groundwater velocity, which is held constant at all depths in our simulations based on the specified hydraulic gradient, hydraulic conductivity, and porosity. Below the hyporheic zone, the thermal dispersion of groundwater was neglected by setting $D_T = 0$ in VS2DH.

[20] Within the hyporheic zone in VS2DH, we set the value of thermal dispersion (D_T) to achieve a specific hyporheic flux as follows. Hydrodynamic dispersion of heat can be related to hyporheic water flux through a first-order mass transfer model of dispersive transport into a layer of specified thickness. The mass transfer coefficient α_{eff} [t^{-1}] for one-dimensional (layered) transport equals $\pi^2 D_e/4a^2$ [*Haggerty and Gorelick*, 1995], where D_e is an effective diffusion coefficient for bulk sediment and $2a$ is the distance from the surface to the depth of the sediment layer (either the depth of the hyporheic zone or the depth of sensors used to quantify hyporheic flow). To compute the hyporheic flux of stream water into a unit surface area of streambed, the mass transfer coefficient α_{eff} is multiplied by the equivalent depth of stream water in the sediment layer, $2a \cdot \theta \cdot f_h$, to give

$$q_{hyp} = \theta f_h \frac{\pi^2 D_e}{2a} \tag{3}$$

where f_h is the fraction of water in the hyporheic zone derived from stream water (rather than from groundwater). The average residence time, t_h, of hyporheic flow is the equivalent depth of surface water in the sediment layer divided by the hyporheic flux, $(2a \cdot \theta \cdot f_h)/q_{hyp}$, which equals $4a^2/(\pi^2 D_e)$, i.e., the inverse of the mass transfer coefficient. Note that for the present application to heat tracing of hyporheic flow, we substitute D_T, the coefficient for thermal dispersion of heat, for the value of D_e in the mass transfer relationship.

[21] To use equation (3) an estimate of the depth of the hyporheic zone ($2a$) is needed. Solute tracer injections in the stream and measurement in the bed provide precise measurements of the depth of stream water penetration and the fraction of stream water in those flow paths (f_h usually near 1) [see *Fuller and Harvey*, 2000]. This paper indicates that heat transport modeling may provide an approximate estimate of hyporheic zone depth as the vertical distance over which enhanced dispersion of heat is apparent. For simple bed forms, an alternative estimate of hyporheic zone depth can be made from average bed form geometry, with hyporheic zone depth scaling approximately with 0.8 times the bed form wavelength [*Cardenas and Wilson*, 2007; *Elliott and Brooks*, 1997a].

[22] Six model scenarios were tested: combinations of two groundwater fluxes (upward or downward) and three dispersivity values corresponding to no, slow, or fast hyporheic flow. The six scenarios are summarized in Table 2. In cases with hyporheic flow, the maximum depth of hyporheic flow paths was chosen to be 7 cm to produce reasonable fluxes and residence times for both slow and fast hyporheic conditions. Models 1, 2, and 3 have upward groundwater fluxes, and models 4, 5, and 6 have downward groundwater fluxes, both with magnitudes of 1×10^{-6} m/s. Models 1 and 4 have no hyporheic flow ($D_T = 0$ throughout), models 2 and 5 have slow hyporheic flow with hyporheic residence times of 1.7 h, and models 3 and 6 have fast hyporheic flow with residence times of 10 min.

Table 2. Numerical Experiments Completed Using VS2DH and Groundwater and Hyporheic Fluxes Used[a]

Model	1	2	3	4	5	6
Groundwater flow direction	Up	Up	Up	Down	Down	Down
Hyporheic flow paths	None	Slow	Fast	None	Slow	Fast
Groundwater flux q_{gw} (m/s)	-1×10^{-6}	-1×10^{-6}	-1×10^{-6}	1×10^{-6}	1×10^{-6}	1×10^{-6}
Hydraulic conductivity K (m/s)	1×10^{-4}	1×10^{-4}	1×10^{-4}	1×10^{-4}	1×10^{-4}	1×10^{-4}
Hydraulic head gradient (–)	-1×10^{-2}	-1×10^{-2}	-1×10^{-2}	1×10^{-2}	1×10^{-2}	1×10^{-2}
Porosity θ (–)	0.4	0.4	0.4	0.4	0.4	0.4
Linear velocity q_{gw}/θ (m/s)	-2.5×10^{-6}	-2.5×10^{-6}	-2.5×10^{-6}	2.5×10^{-6}	2.5×10^{-6}	2.5×10^{-6}
Thermal dispersion D_T (m^2/s)	0	1×10^{-7}	1×10^{-6}	0	1×10^{-7}	1×10^{-6}
Hyporheic depth $2a$ (m)	0	0.07	0.07	0	0.07	0.07
Hyporheic flux q_{hyp} (m/s)	0	4.5×10^{-6}	4.5×10^{-5}	0	4.5×10^{-6}	4.5×10^{-5}
Residence time t (min)	NA	100	10	NA	100	10
Residence time t (hours)	NA	1.7	2×10^{-1}	NA	1.7	2×10^{-1}

[a]Positive groundwater fluxes are downward.

3.2. Field Application at Clear Run, North Carolina

[23] Clear Run is a second-order stream in Wilmington, North Carolina, in the Atlantic Coastal Plain. Its drainage area of 24 km^2 includes the campus of the University of North Carolina Wilmington and is 23% impervious. Clear Run is a tributary to Bradley Creek, a tidally influenced stream draining to Masonboro Sound. Clear Run is relatively narrow (3 m), shallow (6 cm), and fast flowing (20 cm/s). The streambed sediments are composed of sand with a geometric-mean grain size of 0.38 mm. The primary bed forms in Clear Run during base flow were dunes approximately 12 cm in length and 1.5 cm high. Sandbars were present, although not abundant in the stream, and larger-scale roughness features, such as riffles or wood debris in the stream, were rare and entirely absent in our study reach. The stream is susceptible to flooding year round with overbank flows typically occurring during the onshore movement of extratropical storms. Precipitation events can cause spikes in stream temperature due to the stormflow contribution of hot, impervious surfaces. During the study period in September and October of 2009, there was a period of major flooding caused by a strong convective event that produced significant rainfall. Bankfull flow occurred in Clear Run in two distinct events separated by approximately 1 day.

3.2.1. Streambed Temperature and Pressure Transducer Measurements at Clear Run

[24] Temperature was measured in the surface of the stream and within the streambed at depths of 7.6, 15.2, and 25.4 cm. Temperature was measured using iButton temperature loggers (DS1922L; Maxim/Dallas Semiconductor, Dallas, TX), which have a resolution of 0.0625°C and an accuracy of 0.5°C. The temperature loggers were epoxied to a PVC strip, which was pushed into the sandy streambed in the center of the stream channel. Temperature was sampled at an interval ranging from 3 to 10 min between 14 September 2009 and 2 October 2009. Pressure transducers (HOBO U20 Water level data logger; Onset Corp., Bourne, MA) were deployed into 1″ nominal piezometers in the stream, stream bank, and 61 cm below the streambed. The sampling interval was 1 min, and the transducers have an accuracy of 0.5 cm. The transducers also collected temperature data with an accuracy of 0.37°C and a resolution of 0.1°C. Water-level data, which were used along with surveyed elevations to calculate hydraulic head, were collected 17–21 September 2009 and 23 September to 4 October 2009, although the surface water transducer did not produce data during the first time period. Portions of the data from these two time periods are used to examine stream behavior during base flow and storm conditions, respectively.

3.2.2. Streambed Physical Measurements at Clear Run

[25] The streambed was cored to a depth of 10 cm using clear polycarbonate cylinders (nominally 0.048 m internal diameter with 0.00159 m wall) that had been sharpened at one end. Slug tests were performed to estimate sediment hydraulic conductivity using approaches outlined in detail by *Landon et al.* [2001] and *Reynolds et al.* [2002]. From those measurements, a mean hydraulic conductivity was determined with a 95% confidence interval of approximately ±66%. Core tubes used for slug tests were removed with intact sediments, immediately extruded, sectioned into 1 cm increments, bagged, and returned to the laboratory to be dried to a constant weight in a 60°C oven for determination of porosity and grain-size distribution by dry sieving.

3.2.3. Estimating Vertical Fluxes at Clear Run Using VS2DH

[26] The base flow period (16–22 September 2009) and the storms (25–27 September 2009) were separately simulated in VS2DH. The domain was one-dimensional and 61 cm in depth. The surface boundary condition was constant hydraulic head of 0 m and measured surface water temperatures, resampled to a uniform time step of 1 min. In our case, the water levels measured at the stream surface and at a depth of 61 cm differed only slightly (0.6 cm) and are subject to transducer measurement error and surveying error. Because measured differences in water level were small compared to instrument accuracy, groundwater flux was estimated as a calibration parameter during both base flow and stormflow simulations in VS2DH. Therefore, the bottom boundary condition was constant hydraulic head, varied as a calibration parameter, and temperature equal to that measured by the bottom pressure transducer. The initial conditions used were hydraulic head and temperature corresponding to the groundwater flux used in that simulation and initial temperatures, applied at the depths at which they were measured. The thermal parameters for the base flow simulations were homogeneous throughout the domain and are given in Table 1. The parameters used in the storm simulations are the same as given in Table 1, except for dispersion, which was used to simulate increased hyporheic flux during the storm event.

3.2.4. Estimating Vertical Fluxes at Clear Run Using the Thermal Analytical Method

[27] Temperature data were used to calculate vertical fluxes using the commonly used thermal analytical method of *Hatch et al.* [2006]. Filtering was not used because of the short record length, and the method was only applied to the base flow period (16–22 September 2009). The analytical method could not be used during the storm period because diel cycles with a regular periodicity in temperature at depth were not evident. Depths on days without obvious minimum or maximum temperatures were excluded. The parameters used for the analytical method are given in Table 1.

3.2.5. Hydrologic Tracer Experiment in Clear Run

[28] The temperature analysis is supplemented and compared with hyporheic flow-path depths, fluxes, and residence times obtained from a hydrologic tracer experiment. This experiment was conducted on 18 September 2009 in Clear Run and consisted of an in-stream injection of a conservative solute (KBr). The injection lasted for 3.5 h during clear, calm weather with steady base flow discharge in the stream (0.06 m^3/s). In addition to in-stream concentrations of the solute tracer, we simultaneously collected subsurface samples for tracer analysis by slow pumping of small-volume samples for 8 h from depths of 1.5–75 cm below the streambed using the methods of *Harvey and Fuller* [1998]. Tracer modeling analysis followed the detailed guidelines presented in *Harvey and Wagner* [2000], *Harvey and Fuller* [1998], and *O'Connor and Harvey* [2008].

4. Results

4.1. Threshold for Interactions Between Hyporheic and Groundwater Fluxes

[29] *Cardenas and Wilson* [2007] show how hyporheic fluxes vary with Reynolds number of streamflow, ambient

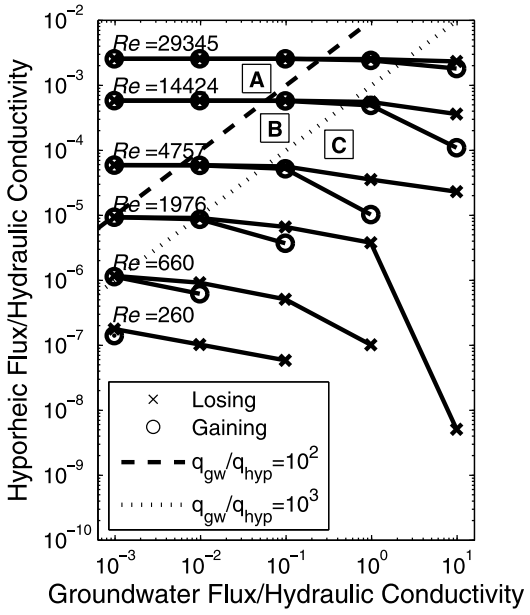

Figure 2. Sensitivity of bed form-scale hyporheic flux to changes in groundwater flux. Scaled groundwater and hyporheic fluxes are shown for different Reynolds numbers of surface water flow, using data plotted in Figures 3 and 5 of *Cardenas and Wilson* [2007] (B. Cardenas, personal communication, 2011). The Reynolds number, *Re*, is defined as $\frac{U_{ave}h}{\nu_f}$, where U_{ave} is average surface water velocity, h is bed form height, and ν_f is fluid kinematic viscosity [*Cardenas and Wilson*, 2007]. Region A (left of the dashed line) indicates a region where hyporheic flux is unaffected by changes in groundwater flux. Region B (between the dashed and dotted lines) indicates the threshold region. Region C (right of the dotted line) indicates a region where hyporheic flux is strongly affected by changes in groundwater flux.

groundwater condition, and bed form geometry. These same data, plotted in Figures 3 and 5 of that paper [*B. Cardenas, personal communication*, 2011], were used in our study to compare groundwater and hyporheic fluxes as they vary across a range of Reynolds numbers. The relationship between scaled groundwater and hyporheic fluxes, which we determined from reanalysis of simulations from *Cardenas and Wilson* [2007], is shown in Figure 2. The Reynolds number from *Cardenas and Wilson* [2007] is defined as $Re = \frac{U_{ave}h}{\nu_f}$, where U_{ave} is average water column velocity, h is bed form height, and ν_f is fluid kinematic viscosity. We used the bed form geometry from their work that is most similar to bed form dunes such as those at the Clear Run site, which has a ratio of bed form height to length of 0.075.

[30] Figure 2 shows that as the Reynolds number increased, hyporheic fluxes also increased, because larger bed forms and higher stream velocities drove greater hyporheic exchange. Furthermore, as vertical groundwater fluxes increased, hyporheic fluxes decreased, at first gradually and later steeply, after about $q_{gw}/q_{hyp} > 1000$. Below the threshold region, any increase in groundwater fluxes (even when groundwater fluxes were 10-fold greater than hyporheic fluxes) produced little change in the magnitude of hyporheic fluxes (Figure 2). The dependence of hyporheic fluxes on groundwater fluxes was similar but was more pronounced for gaining compared with losing groundwater conditions.

4.2. Hyporheic and Groundwater Interactions Using the Thermal Analytical Method

[31] Vertical flux as calculated using the thermal analytical method for specified combinations of groundwater and hyporheic fluxes in one-dimensional numerical experiments is here called "apparent flux." Figure 3 shows the apparent flux calculated using the analytical method for the six model scenarios given in Table 2. In Figure 3, calculated apparent

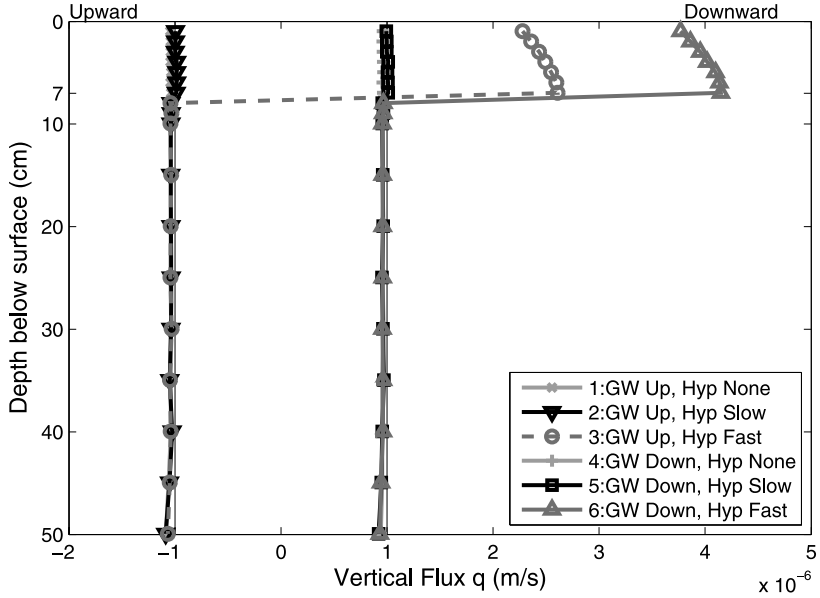

Figure 3. Downward flux with depth of VS2DH numerical experiments as calculated by the *Hatch et al.* [2006] thermal analytical method. Numbers in the legend refer to six scenarios given in Table 2. Vertical black lines indicate the constant upward or downward groundwater flux specified. Note that hyporheic flux was specified as bidirectional, using thermal dispersion.

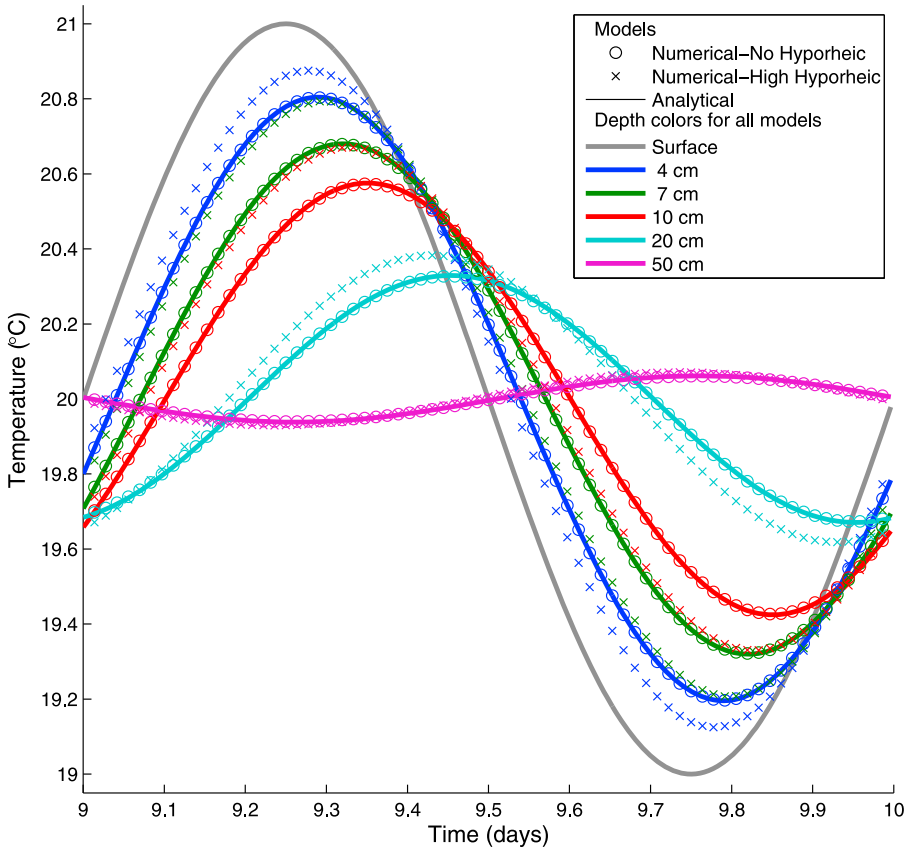

Figure 4. Temperature time series at various depths below the streambed (1) from the analytical method for a groundwater flux of 1×10^{-6} m/s (plotted in solid lines); (2) simulated by the numerical experiment VS2DH model 4, which has a groundwater flux of 1×10^{-6} m/s and no hyporheic flux (plotted with open circles); and (3) simulated by the numerical experiment VS2DH model 6, which has a groundwater flux of 1×10^{-6} m/s and fast hyporheic flux within the top 7 cm (plotted with closed dots). Note only every other marker for the numerical model was plotted shown so that the analytical solution can also been seen.

fluxes for both simulations without a hyporheic zone were within 4% of the groundwater fluxes specified.

[32] For scenarios with hyporheic exchange, the depth of the hyporheic zone was 7 cm. The slow hyporheic scenarios have an apparent flux slightly greater (5×10^{-8} m/s or 5%) in the top 7 cm compared to the groundwater-only scenarios, regardless of whether groundwater flow is upward or downward. The fast hyporheic scenarios, for both upward and downward groundwater flow, had apparent fluxes within the top 7 cm which were 3×10^{-6} m/s (300%) greater than that of the specified groundwater flux alone. Even in this fast hyporheic case, however, in which the hyporheic flux (4.5×10^{-5} m/s) was 1 order of magnitude greater than the groundwater flux specified, the apparent flux within the top 7 cm does not equal the specified hyporheic flux. Instead, the shallow flux value is between the specified hyporheic and groundwater fluxes, possibly showing sensitivity to both because the hyporheic flux was not large enough to overwhelm the groundwater flux.

[33] The relative strengths of the two fluxes for our different numerical experiments may be quantified using the thermal diffusivity index, which is the ratio of thermal dispersion to thermal conduction $\left(\frac{D_T}{\frac{\lambda}{C}}\right)$. The numerator indicates the thermal dispersion which leads to hyporheic flux, whereas the denominator indicates the strength of thermal conduction countering the detection of hyporheic flux. For the no hyporheic flow models, this ratio equaled 0; for the slow hyporheic flow models, the ratio equaled 0.05; and for the fast hyporheic flow models, the ratio equaled 0.5. In the fast hyporheic simulations, the ratio indicates that thermal dispersion is considerable, and hyporheic flux significantly influences the vertical fluid flux as quantified with the thermal analytical method, but thermal conduction still dominates the overall thermal diffusivity term.

[34] In Figure 3, we compared the flux estimates specified in the numerical experiments with those calculated using the analytical method. We can also compare simulated temperature series with time series predicted by the analytical method for a specified groundwater flux. Simulated and analytical temperature time series at selected depths are shown in Figure 4.

4.3. Clear Run Field Interpretation of Co-occurring Hyporheic and Groundwater Fluxes

4.3.1. Streambed Fluxes at Clear Run During Base Flow

[35] We simulated temperature measurements at Clear Run using VS2DH, which allows for variable thermal dispersion with depth. Simulated and measured temperature during base flow conditions are shown in Figure 5. The

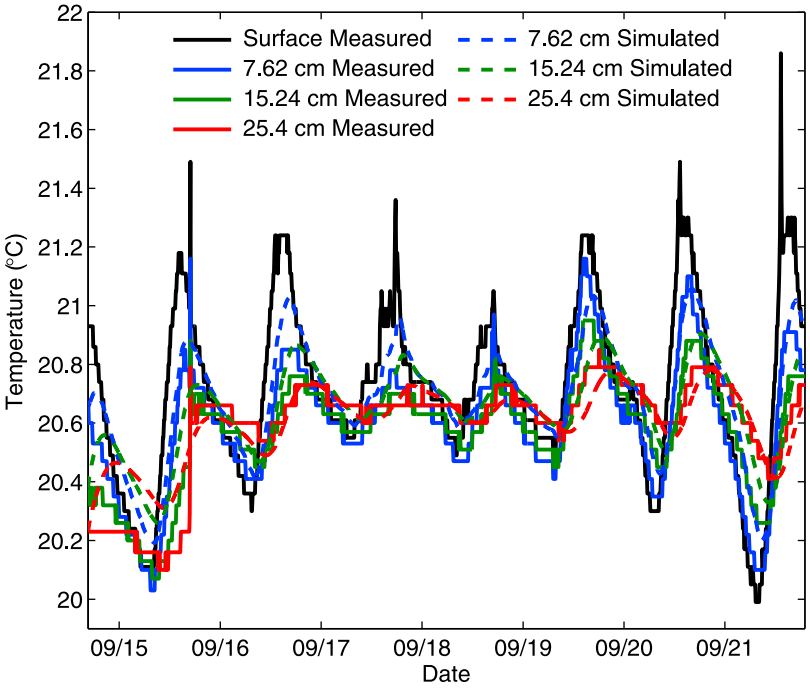

Figure 5. VS2DH simulated and measured temperature data during base flow conditions in Clear Run. With a calibrated vertical flux of 1×10^{-6} m/s, root mean square error (RMSE) is 0.1°C.

calibrated vertical flux used in the simulation was 1×10^{-6} m/s. Hyporheic flux, simulated by shallow dispersion, was not needed to fit measured temperature curves in the base flow simulations. The diel surface temperature was transported into the subsurface by downward groundwater flow and heat conduction. The depth of hyporheic exchange was determined to be 6.4 cm based on solute tracer methods. We therefore could not expect that our shallowest temperature measurement at 7.6 cm would have been sensitive enough to detect hyporheic fluxes during base flow conditions at Clear Run. The model was effective only in quantifying groundwater flow during base flow.

[36] The thermal analytical method has seen wide usage and was also used during base flow to determine vertical groundwater fluxes. For a given set of thermal and hydraulic parameters, there is a known relationship between amplitude ratio and vertical flux. The relationship between amplitude ratio and vertical flux (equation (2)) for the parameters in Table 1 and relevant sensor pair spacing is shown in Figure 6 [after *Hatch et al.*, 2006]. Also shown in Figure 6 are data points representing the amplitude ratio and corresponding vertical flux during base flow in Clear Run using temperature measurements from each pair of adjacent sensors. Because the analytical method is based on the ratio of daily temperature amplitudes, there is a data point for each depth pair on each day of the study period. The fluxes between the two deepest pairs of sensors (7.6 and 15.2 cm; 15.2 and 25.4 cm) were averaged across all days to determine a vertical flux of groundwater equal to 3×10^{-7} m/s.

[37] We independently estimated the hyporheic flux during base flow using data from the tracer experiment. The flux-weighted hyporheic flux was found to be 1×10^{-5} m/s, and the depth of hyporheic flow paths was found to be 6.4 cm. We also used a second method to estimate hyporheic flux during base flow. Field measurements of streamflow velocity, stream depth, bed form geometry, particle size, and permeability were used in the scaling relationship of *O'Connor and Harvey* [2008] to calculate the effective diffusion coefficient [*O'Connor and Harvey*, 2008, equation (35)]. The effective diffusion coefficient was then used to calculate hyporheic flux with equation (3), using hyporheic zone depth (6.4 cm), porosity of sediment (0.4), and fraction stream water in the hyporheic zone (1) estimated from the solute tracer experiment. The resulting hyporheic flux during base flow using this method was 9×10^{-6} m/s.

4.3.2. Streambed Fluxes at Clear Run During Stormflow

[38] During 25–28 September 2009, there were two rain events clearly visible as spikes in the surface temperature data of Clear Run (Figure 7). Whereas the stream temperature during base flow had daily maximum values less than 22°C (Figure 5), stream temperature was as high as 27°C during the storm (Figure 7). This was likely due to fast overland flow and storm drain inputs from hot, impervious surfaces in the Clear Run watershed. Water-level data indicated the second stormflow response was larger in magnitude (data not shown), but the temperature spike was much higher for the first storm, possibly because impervious surfaces were cooled by the first storm. The presence of these temperature spikes overwhelmed the diel temperature signal and therefore did not allow the use of the standard thermal analytical method, which is normally used to analyze sinusoidal, diel temperature variations. The storm temperatures were simulated in VS2DH and are shown along with measured temperatures in Figure 7.

[39] During stormflow, the measured temperature at all depths could not be simultaneously matched by using the value of vertical groundwater flux as the only calibration parameter. Whereas a lower groundwater flux value provides a better match to the deepest (25.4 cm) temperature

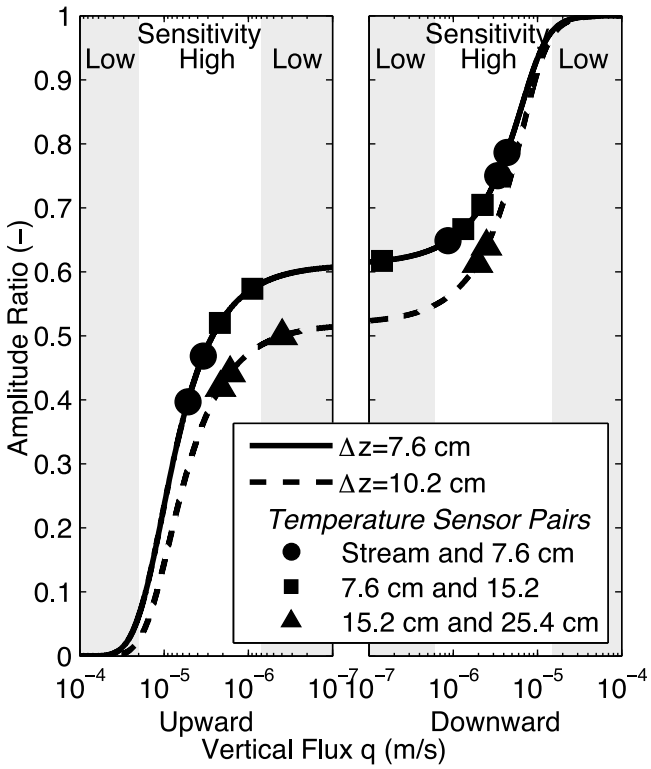

Figure 6. Sensitivity plot of streambed flux versus amplitude based on the analytical method of *Hatch et al.* [2006] for two different sensor spacings at Clear Run (solid and dashed lines). Also plotted are the amplitude ratios and associated fluxes for sensor pairs over 3 days at Clear Run during base flow. The upward fluxes are negative and downward are positive, and they are separated because of the semi-log plot used. Unshaded areas are the approximate limits of high sensitivity of the analytical method for the measurements at Clear Run.

measurement (Figure 7b), a higher groundwater flux value better matches the two shallower (7.6 and 15.2 cm) temperature measurements (Figure 7a). Our interpretation of the mismatch between simulated and measured temperature is that hyporheic and groundwater fluxes were co-occurring and that shallower sensors were more sensitive to hyporheic flow. During storm conditions, the height of bed forms and stream velocity increased, which can be expected to lead to larger-magnitude hyporheic fluxes and an increased depth of hyporheic flow paths.

[40] Therefore, we attempted to improve the simulation by introducing hyporheic flow in the form of a zone of increased shallow dispersion. From the model calibration perspective, this approach increases the likelihood of finding a nonunique fit to the data, since both dispersion and flux are used as calibration parameters. Formally addressing nonuniqueness in hydrologic models is an area of active research [e.g., *Beven*, 2008] that it is beyond the scope of the present investigation. Here we simply demonstrate that introducing a hyporheic zone to the model in the form of increased dispersion at shallow depths can better match temperatures at all depths as compared to a model with constant vertical fluid flux (Figure 7). In this case, the shallowest layer (0–7.6 cm) was matched with higher thermal dispersion (D_T = 8 × 10^{-6} m^2/s) compared with the intermediate (7.6–15.2 cm) hyporheic layer (D_T = 3 × 10^{-7} m^2/s) and deeper layer (15.2–25.4 cm) without hyporheic flow (D_T = 0 m^2/s).

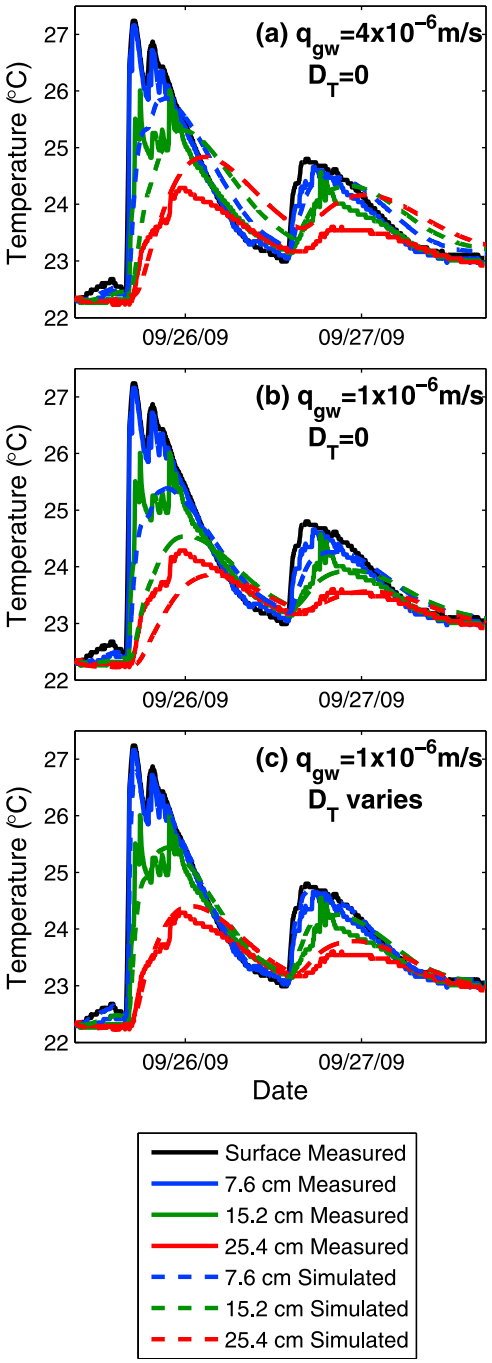

Figure 7. VS2DH simulated and measured temperatures during storm conditions in Clear Run. (a) A model calibrated with a groundwater flux of 4 × 10^{-6} m/s. (b) A model calibrated with a groundwater flux of 1 × 10^{-6} m/s. (c) A model calibrated with a groundwater flux of 1 × 10^{-6} m/s and depth-variable dispersion: stream to 7.6 cm depth had thermal dispersion D_T = 8 × 10^{-6} m^2/s; 7.6–15.2 cm had D_T = 3 × 10^{-7} m^2/s; deeper had a D_T = 0 m^2/s. Root mean square error (RMSE) for Figures 7a–7c were 0.53, 0.51, and 0.19°C, respectively.

We found a reasonable fit (Figure 7c) to temperature data at all depths using a constant groundwater flux of 1×10^{-6} m/s, the same value used in the base flow simulations. For comparison, Figure 7b uses this same groundwater flux but without increased shallow dispersion.

[41] Similar to the analysis performed with the numerical experiments, we can calculate the thermal diffusivity index $\left(\frac{D_T}{\frac{\lambda}{C}}\right)$ for the storm simulation. The shallowest layer (0–7.6 cm) has a ratio of 4, and the deeper layer (7.6–15.2 cm) has a ratio of 0.1, suggesting that heat transport by dispersion is more significant than that of thermal conduction between depths of 0 and 7.6 cm in the streambed, making the hyporheic flux easily detectable in the shallow part of the hyporheic zone. Hyporheic flux was smaller in the deeper part of the hyporheic zone between 7.6 and 15.2 cm, and the deepest depths are well matched with no hyporheic flow.

[42] We can also use the thermal diffusivity index to calculate the limits of detection of hyporheic flux, assuming that hyporheic exchange is detectable when the thermal diffusivity index takes on a certain value (here called the detection limit ratio). We choose the detection limit ratio to be 1, meaning that we consider hyporheic flux to be detectable when the heat transport signal of thermal dispersion due to hyporheic exchange is equal to or greater than thermal conduction. The minimum detectable hyporheic flux can be found by rearranging the thermal diffusivity index $\left(\frac{D_T}{\frac{\lambda}{C}}\right)$ and using the relationship between hyporheic flux and dispersion given in equation (3):

$$\text{detectable } q_{hyp} = \frac{\theta\ f_h\ \pi^2\ \lambda(\text{detection limit ratio})}{2a\ C} \qquad (4)$$

where we pick the detection limit ratio = 1. Given the parameters in Table 1, we calculate the minimum detectable hyporheic fluxes corresponding to the exchange depths of 2, 7, and 15 cm using equation (4) to be 2×10^{-4}, 5×10^{-5}, and 2×10^{-5} m/s, respectively. These are the approximate minimum values of hyporheic flux that would be detectable as demarcated by a threshold where thermal dispersion and conduction play equal roles in thermal diffusivity. Note that these approximate minimum thresholds for detecting hyporheic fluxes are large relative to the range of typical sensitivity of the thermal analytical method to detect vertical fluxes shown in Figure 6 and also large relative to hyporheic fluxes considered in the numerical simulations, except in the storm case.

5. Discussion

5.1. Implications for Co-occurring Hyporheic and Groundwater Fluxes

[43] Hyporheic fluxes typically co-occur with groundwater fluxes in permeable streambeds. Reexamination of results from *Cardenas and Wilson* [2007] makes apparent that hyporheic fluxes are relatively independent of and can co-occur with groundwater fluxes until groundwater fluxes become orders of magnitude larger. That hyporheic fluxes remain independent of groundwater fluxes until this relatively high threshold may indicate the dominance of nearby current-driven forcing, as compared to the hydraulic head gradient forcing in the larger system. It should be noted that unlike hyporheic fluxes, which are insensitive except to relatively high values of groundwater fluxes, the depth of the hyporheic flow in the streambed is more sensitive to groundwater control when hyporheic and groundwater fluxes are relatively similar [Figure 3 in *Cardenas and Wilson*, 2007].

[44] The possibility of frequently co-occurring hyporheic and groundwater fluxes has a number of biochemical implications, such as increased contact time and contact area for a mixture of surface and subsurface waters, with very different chemical compositions, in the shallow streambed. This mixing in the hyporheic zone between surface and subsurface waters favors enhancement and biogeochemical processing of carbon, nutrients, and contaminants [*Fanelli and Lautz*, 2008; *Fuller and Harvey*, 2000; *Hedin et al.*, 1998]. The extended analysis of temperature advanced here increases the understanding of co-occurring hyporheic and groundwater fluxes.

5.2. Dynamic Surface-Subsurface Water Interactions

[45] Most studies of groundwater-surface water interactions have investigated fluxes during base flow conditions, but we cannot assume these fluxes remain constant in space or time. Hyporheic flow may frequently change during storm conditions. For example, larger stream velocities can drive stream water deeper and faster, and bed form wavelength can increase during floods. Groundwater fluxes can change magnitude and even direction during storm conditions. For example, the initial channel flood wave may increase downward fluxes whereas later groundwater contributions to stormflow may increase upward fluxes. Estimates of groundwater-surface water fluxes during storms are important for understanding stormflow generation and biogeochemical processing of stormflow solute load in the hyporheic zone. This study sought to estimate temporally varying bed form-driven hyporheic flux using heat as a tracer.

[46] The use of heat as a tracer is well suited to calculate hyporheic and groundwater fluxes during storm events. The equipment can be left in the stream during a wide range of flow conditions, the sensors provide almost instantaneous measurements as compared to solute tracing, and the method is not subject to the large uncertainty in hydraulic conductivity as in Darcy flux estimates. We found that at the Clear Run field site, the hyporheic flow paths increased in depth (from approximately 6 cm to 15 cm) between base flow and storm conditions and hyporheic flux increased by 1 order of magnitude (Table 3). The increased hyporheic flux during storm events as compared to base flow time periods, with a greater volume of water entering hyporheic flow paths and increased residence times, could lead to increased storage of solutes that buffer storm-driven exports. More research will be needed to substantiate these initial findings.

5.3. Apparent Nonconstant Vertical Flux in Heat Tracing of Streambed Fluxes

[47] A number of researchers have commented on the apparent nonconstant vertical flow indicated by heat tracing in streambeds [*Briggs et al.*, 2012; *Lautz et al.*, 2010; *Swanson and Cardenas*, 2010]. Our simulations indicate that co-occurrence of bed form-scale hyporheic and groundwater flow provides one possible explanation for those

Table 3. Co-occurring Groundwater and Hyporheic Fluxes Estimated for Base Flow and During a Bankfull Flood in Clear Run, North Carolina[a]

Time Period	Flux Type	Flux Value (m/s)	Method
Base flow	Groundwater	3×10^{-7}	Analytical method of *Hatch et al.* [2006]
Base flow	Groundwater	1×10^{-6}	Calibration of flux in VS2DH simulation
Base flow	Hyporheic	9×10^{-6}	Using effective diffusion coefficient calculated from *O'Connor and Harvey* [2008] and equation (3)
Base flow	Hyporheic	1×10^{-5}	In-stream solute tracer test with simultaneous subsurface measurements [following *Harvey and Fuller*, 1998]
Storm	Groundwater	1×10^{-6}	Calibration of flux in VS2DH simulation
Storm	Hyporheic	5×10^{-4} (0–7.6 cm)	Calibration of flux in VS2DH simulation, where the parenthetical values indicate hyporheic depth
		1×10^{-5} (7.6–15.2 cm)	

[a]Positive groundwater fluxes are downward, losing, and recharging.

observations. We analyzed numerical simulations with co-occurring hyporheic and groundwater fluxes using the thermal analytical method and found vertically nonconstant apparent flux (Figure 3). Flow was strictly vertical in our numerical experiments, and thus our simulations show that the vertically nonconstant apparent flux calculated with the thermal analytical method can arise solely to one-dimensional advection and dispersion of heat. Although net water flux was constant with depth in all of our simulations, thermal transport is not constant with depth because of the enhanced dispersion in the hyporheic zone dominating transport in a layer just beneath the streambed, with a unidirectional groundwater flux dominating transport beneath the hyporheic layer. Specifically, we use measurements of depth-variable thermal transport to quantify a dispersive exchange flux of water, which is the hyporheic component of streambed flux.

[48] Because of nonconstant vertical heat transport, the depth of deployment of temperature sensors can substantially affect modeling results. For example, the presence of hyporheic flow not only affects temperature dynamics in the hyporheic zone but also affects deeper temperature dynamics (Figure 4). The temperature observations from the VS2DH numerical experiment with no hyporheic flow (open circles) showed excellent agreement with the temperature time series derived using the analytical expressions in *Hatch et al.* [2006] (solid lines) (Figure 4). As we might expect, the temperature predicted by the analytical method does not match temperature from the VS2DH simulation with fast hyporheic flow in the top 7 cm. However, note that the mismatch between the analytical method and the VS2DH simulation with fast hyporheic flow extends to 50 cm, even though the hyporheic zone only is 7 cm deep. This phenomenon was also observed during temperature simulation of the Clear Run storm, where the introduction of increased dispersion at shallow depths led to temperature shifts at deeper depths (compare the deepest sensor in Figures 7b and 7c).

[49] As a result of the above discussion, the choice of spacing between temperature sensors is important, especially where the goal is to independently estimate hyporheic and groundwater fluxes. Figure 3 shows that the flux estimated in the fast hyporheic case is in agreement with the specified groundwater flux for observation points deeper than the hyporheic zone. This is because analytical method fluxes were calculated using adjacent neighboring pairs of observation points, which are all affected by shallow dispersion. However, if temperature records from below the hyporheic zone were paired instead with stream temperature, which is not affected by shallow dispersion, the groundwater flux estimate from the analytical method would reflect the combined effects of vertical fluid flux due to groundwater as well as thermal dispersion due to hyporheic flow. The pairing of stream and groundwater temperature records in the analytical method would therefore not provide an accurate estimate of groundwater flux. Whether the aim is to estimate both groundwater and hyporheic fluxes or to isolate one or the other, temperature sensors need to be placed appropriately using guidance such as scaling of hyporheic zone depth with bed form wavelength. At a minimum, several sensors in the expected range of hyporheic zone depth and several sensors beneath that are needed if the goal is to quantify both types of fluxes.

5.4. Comparison of Streambed Fluxes Estimated by Different Field Methods

[50] Hyporheic fluxes were estimated to be 1–2 orders of magnitude greater than groundwater fluxes during both base flow and stormflow conditions at Clear Run. Where vertically variable estimates were made, the shallower hyporheic fluxes were found to be larger in magnitude than the deeper hyporheic fluxes. The fluxes calculated at Clear Run during different streamflow conditions and by different methods are summarized in Table 3. During base flow, the two estimates of groundwater flux are within 1 order of magnitude of each other, as are the two estimates of hyporheic flux.

[51] The flux estimates compared in Table 3 are subject to multiple sources of error. The calibration of flux in VS2DH is subject to errors because (1) flux was assumed to be temporally constant in the calibration, due to the lack of precise hydraulic head measurements; (2) hydraulic conductivity was assumed to be uniform; (3) initial conditions may have a disproportionate impact on the short time periods simulated; (4) calibration was done by trial and error; and (5) one-dimensional temperature data were used in the one-dimensional model domain, although flow likely does not occur only in the vertical direction. Especially during storms, it is unreasonable to assume that streambed fluxes were constant. Despite these limitations, we have demonstrated that by including thermal dispersion within the hyporheic zone, we have much improved the match between the simulation results and field data. A time-varying simulation of streambed fluxes is beyond the scope of this work but would be aided by more precise measurements of hydraulic gradient that would allow us to better define the groundwater flux.

[52] Errors of the thermal analytical method can result from (1) the limited range of sensitivity of the method and (2) violations of assumptions of the analytical solution. *Hatch et al.* [2006] stated that the amplitude ratio thermal analytical method is most sensitive to fluxes near 0, specifically between 5.8×10^{-5} and -2.7×10^{-5} m/s for their thermal parameters. The downward hyporheic fluxes found during the storm in Clear Run (on the order of 10^{-4} m/s; Table 3) would fall along the flat upper part of the curve shown in Figure 6. Because of the low sensitivity of the method in that portion of the curve, Clear Run hyporheic fluxes are too fast to be determined with precision using the analytical method, even though the hyporheic exchange was captured by temperature measurements. Violations of the assumptions of the analytical method, such as a horizontal component of flow, can also lead to large errors [*Lautz*, 2010] but was not evaluated here since the temperature sensors were placed in a vertical array. The analytical method is steady state but produces a flux estimate for each day and sensor pair used, which can vary over multiple orders of magnitude (Figure 6). *Lautz* [2010] recommends using the average of fluxes over multiple days, but some researchers have treated each daily flux as an independent estimate and used the analytical method to determine transient fluxes. It is not clear whether or when the analytical method is robust under conditions of changing vertical flux. Application of the thermal analytical method to a site 0.2 km upstream on Clear Run showed that groundwater was discharging, as opposed to the recharging conditions found at this study site. In addition to varying over space, we found that vertical fluxes and hyporheic conditions at the same location also vary strongly in time. Further work needs to be done to examine the errors of the thermal analytical method with violations of the steady, uniform flow assumptions. VS2DH is able to incorporate temporally varying flux but requires accurate measurements of hydraulic conductivity and hydraulic head.

6. Conclusions

[53] Hyporheic fluxes generally co-occur with groundwater fluxes beneath bed forms in permeable sediments of flowing water bodies. Based on reanalysis of numerical simulations by *Cardenas and Wilson* [2007], the magnitude of hyporheic and groundwater fluxes are largely independent of one another until a threshold is surpassed where groundwater fluxes exceed hyporheic fluxes by orders of magnitude (100- to 1000-fold). Using heat as a tracer to quantify water fluxes across streambeds has received considerable interest because temperature is inexpensive, easy to measure, robust, and naturally occurring [*Stonestrom and Constantz*, 2003] and because of the potential for temperature tracing to track effects of fluctuating streamflow on streambed water fluxes. However, most applications of heat as a tracer to quantify streambed water fluxes neglect the possibility of co-occurring hyporheic and groundwater fluxes, which may affect the accuracy and interpretation of temperature tracing results.

[54] The present research found that analysis of streambed temperature records can serve to detect different components of the streambed flux, i.e., bidirectional hyporheic fluxes in the shallow streambed as well as the unidirectional exchanges with the deeper groundwater system. To accomplish that, we conceptualized hyporheic flow as shallow enhanced thermal dispersion above a deeper region of recharging or discharging groundwater in a one-dimensional (vertical) domain. Our analysis is an extension of several previous studies, beginning with *Elliott and Brooks* [1997b], who demonstrated that two-dimensional hyporheic advection through the streambed can be analyzed by a one-dimensional (vertical) analysis of effective diffusion.

[55] We began by testing the use of heat as a tracer to quantify both hyporheic and groundwater fluxes using the model VS2DH to conduct numerical simulations of enhanced thermal dispersion above unidirectional groundwater flow. We found that the presence of relatively large hyporheic fluxes can significantly affect the flux calculated using the thermal analytical method of *Hatch et al.* [2006]. When at least one temperature sensor is within the hyporheic zone, and hyporheic flow is relatively fast, the fluxes calculated using the thermal analytical method are affected by both hyporheic and groundwater flow. When the shallowest temperature measurement point is deeper than hyporheic flow paths or when hyporheic flow is slow, the thermal analytical method results in groundwater-dominated calculated fluxes. Whether the ultimate goal of a study is to quantify hyporheic, groundwater, or both fluxes, temperature sensor locations need to be chosen to ensure that the analytical method is sensitive to the desired flux type. To quantify hyporheic fluxes, it is necessary to have a preliminary estimate of hyporheic depth to ensure the shallowest temperature sensor is within the hyporheic zone and not primarily sensitive to groundwater fluxes. We also found that to best separate hyporheic flux from deeper groundwater flux using the thermal analytical method, adjacent sensor pairs should be used instead of pairing stream and deeper temperature measurements.

[56] We further tested our conceptualization of co-occurring hyporheic and groundwater flow in the field during both base flow and stormflow conditions at the Clear Run, North Carolina, field site, a sandy Coastal Plain stream. Using a variety of methods, including thermal modeling using VS2DH, the thermal analytical method, a tracer experiment, and the effective diffusion coefficient of *O'Connor and Harvey* [2008], hyporheic fluxes were found to be 1–2 orders of magnitude larger than groundwater fluxes in Clear Run. During base flow, the hyporheic zone was shallow (6.4 cm) and increased (to between 8 and 15 cm) during storms. We found that heat tracing of temporally varying hyporheic and groundwater fluxes through cycles of storms shows great promise, although further work is needed to quantify errors of the thermal analytical method under those conditions.

[57] In summary, we found that the incorporation of both hyporheic and groundwater fluxes in heat transport modeling can be achieved by conceptualizing bed form-scale hyporheic flow as enhanced thermal dispersion. This methodology to include co-occurring hyporheic and groundwater fluxes in the thermal method should broaden capabilities and provide better estimates and interpretation of distinct types of water and biogeochemical fluxes, which will increase overall understanding of groundwater and surface water interactions.

Notation

A_r amplitude ratio $\dfrac{A_{depth}}{A_{shallow}} = \dfrac{T_{depth\,\max} - T_{depth\,\min}}{T_{shallow\,\max} - T_{shallow\,\min}}$ [–].

a distance from sediment surface to mid-depth in sediment layer of mass transfer model, where 2a is the depth of the hyporheic zone [m].

C_s specific heat of dry sediments $\left[\frac{J}{m^3 \circ C}\right]$.

C_w specific heat of water $\left[\frac{J}{m^3 \circ C}\right]$.

C specific heat of water-sediment matrix $\theta C_w + (1\text{-}\theta)C_s$ $\left[\frac{J}{m^3 \circ C}\right]$.

D_e effective diffusion coefficient in bulk sediment $\left[\frac{m^2}{s}\right]$.

D_T thermal hydrodynamic dispersion in bulk sediment $\left[\frac{m^2}{s}\right]$.

f_h volume fraction of water that comprises stream hyporheic flow [−].

H stream depth [m].

h bed form height [m].

K hydraulic conductivity $\left[\frac{m}{s}\right]$.

L bed form wavelength [m].

q vertical fluid flux $\frac{C}{C_w} v$ $\left[\frac{m}{s}\right]$.

q/θ linear vertical velocity $\frac{q}{\theta}$ $\left[\frac{m}{s}\right]$.

Re *Cardenas and Wilson* [2007], Reynolds number $\frac{U_{ave} h}{\nu}$ [−].

S bed slope [–].

T temperature [℃].

t time [s].

t_h median subsurface residence time of hyporheic flow [s].

U_{ave} average water column velocity taken above the crest of the bed form $\left[\frac{m}{s}\right]$.

z depth below the streambed [m].

α term in *Hatch et al.* [2006], thermal analytical equation $\sqrt{\nu^4 + \left(\frac{8\pi\kappa_e}{P}\right)^2}$ $\left[\frac{m}{s}\right]$.

α_{eff} effective mass transfer coefficient for layered diffusion $\left[\frac{1}{s}\right]$.

β thermal dispersivity [m].

θ total porosity [–].

κ_e effective thermal diffusivity $\frac{\lambda}{C} + D_T$ $\left[\frac{m^2}{s}\right]$.

λ thermal conductivity $\left[\frac{J}{ms \circ C}\right]$.

ν thermal front velocity $\frac{C_w}{C} q_{gw}$ $\left[\frac{m}{s}\right]$.

ν_f kinematic viscosity $\left[\frac{m^2}{s}\right]$.

[58] **Acknowledgments.** U.S. Geological Survey hosted ASB for her IGERT internship, providing intellectual mentorship by JWH and EJH, office space and computer resources for three months to carry out this work. We thank J.K. Böhlke, Doug Jerolmack, Aaron Packman, and Craig Tobias for their collaboration in related efforts at Clear Run, Bayani Cardenas for making raw simulation results available from his dissertation and previously published work, and Claire Welty and three anonymous reviewers for helpful and detailed comments on an earlier version of this manuscript. This research was supported by NSF Grants DGE-0549469 "IGERT: Water in the Urban Environment" (ASB), EAR-0810140 (JWH), EAR-0814990 (JWH), a UNCW Cahill Award (EJH), and the USGS HR&D and NAWQA Programs. Any use of trade, firm, or product names is for descriptive purposes only and does not imply endorsement by the U.S. Government.

References

Anderson, M. P. (2005), Heat as a ground water tracer, *Ground Water*, *43*(6), 951–968, doi:10.1111/j.1745-6584.2005.00052.x.

Arrigoni, A. S., G. C. Poole, L. A. K. Mertes, S. J. O'Daniel, W. W. Woessner, and S. A. Thomas (2008), Buffered, lagged, or cooled? Disentangling hyporheic influences on temperature cycles in stream channels, *Water Resour. Res.*, *44*, W09418, doi:10.1029/2007WR006480.

Beschta, R. L. (1997), Riparian shade and stream temperature: An alternative perspective, *Rangelands*, *19*(2), 25–28.

Beven, K. J. (2008), *Environmental Modelling: An Uncertain Future?: An Introduction to Techniques for Uncertainty Estimation in Environmental Prediction*, 328 pp., Routledge, London.

Bianchin, M., L. Smith, and R. Beckie (2010), Quantifying hyporheic exchange in a tidal river using temperature time series, *Water Resour. Res.*, *46*, W07507, doi:10.1029/2009WR008365.

Boano, F., R. Revelli, and L. Ridolfi (2008), Reduction of the hyporheic zone volume due to the stream-aquifer interaction, *Geophys. Res. Lett.*, *35*, L09401, doi:10.1029/2008GL033554.

Boano, F., R. Revelli, and L. Ridolfi (2009), Quantifying the impact of groundwater discharge on the surface-subsurface exchange, *Hydrol. Processes*, *23*, 2108–2116, doi:10.1002/hyp.7278.

Böhlke, J. K., R. C. Antweiler, J. W. Harvey, A. E. Laursen, L. K. Smith, R. L. Smith, and M. A. Voytek (2009), Multi-scale measurements and modeling of denitrification in streams with varying flow and nitrate concentration in the upper Mississippi River basin, USA, *Biogeochemistry*, *93*(1–2), 117–141, doi:10.1007/s10533-008-9282-8.

Bredehoeft, J. D., and B. B. Hanshaw (1968), On the maintenance of anomalous fluid pressures: I. Thick sedimentary sequences, *Geol. Soc. Am. Bull.*, *79*(9), 1097–1106, doi:10.1130/0016-7606(1968)79[1097:OTMOAF]2.0.CO;2.

Briggs, M. A., L. K. Lautz, J. M. McKenzie, R. P. Gordon, and D. K. Hare (2012), Using high-resolution distributed temperature sensing to quantify spatial and temporal variability in vertical hyporheic flux, *Water Resour. Res.*, *48*, W02527, doi:10.1029/2011WR011227.

Caissie, D. (2006), The thermal regime of rivers: A review, *Freshwater Biol.*, *51*(8), 1389–1406, doi:10.1111/j.1365-2427.2006.01597.x.

Cardenas, M. B., and J. L. Wilson (2007), Exchange across a sediment-water interface with ambient groundwater discharge, *J. Hydrol.*, *346*(3–4), 69–80, doi:10.1016/j.jhydrol.2007.08.019.

Conant, B., Jr. (2004), Delineating and quantifying ground water discharge zones using streambed temperatures, *Ground Water*, *42*(2), 243–257, doi:10.1111/j.1745-6584.2004.tb02671.x.

Constantz, J., M. H. Cox, and G. W. Su (2003), Comparison of heat and bromide as ground water tracers near streams, *Ground Water*, *41*(5), 647–656, doi:10.1111/j.1745-6584.2003.tb02403.x.

Elliott, A. H., and N. H. Brooks (1997a), Transfer of nonsorbing solutes to a streambed with bed forms: Theory, *Water Resour. Res.*, *33*(1), 123–136, doi:10.1029/96WR02784.

Elliott, A. H., and N. H. Brooks (1997b), Transfer of nonsorbing solutes to a streambed with bed forms: Laboratory experiments, *Water Resour. Res.*, *33*(1), 137–151, doi:10.1029/96WR02783.

Fanelli, R. M., and L. K. Lautz (2008), Patterns of water, heat, and solute flux through streambeds around small dams, *Ground Water*, *46*(5), 671–687, doi:10.1111/j.1745-6584.2008.00461.x.

Fuller, C. C., and J. W. Harvey (2000), Reactive uptake of trace metals in the hyporheic zone of a mining-contaminated stream, Pinal Creek, Arizona, *Environ. Sci. Technol.*, *34*(7), 1150–1155, doi:10.1021/es990714d.

Galli, J. (1990), Thermal impacts associated with urbanization and stormwater management best management practices, Metropolitan Washington Council of Governments for the Sediment and Stormwater Administration of the Maryland Dept. of the Environment, Washington, D. C.

Gerecht, K. E., M. B. Cardenas, A. J. Guswa, A. H. Sawyer, J. D. Nowinski, and T. E. Swanson (2011), Dynamics of hyporheic flow and heat transport across a bed-to-bank continuum in a large regulated river, *Water Resour. Res.*, *47*, W03524, doi:10.1029/2010WR009794.

Goto, S., M. Yamano, and M. Kinoshita (2005), Thermal response of sediment with vertical fluid flow to periodic temperature variation at the surface, *J. Geophys. Res.*, *110*, B01106, doi:10.1029/2004JB003419.

Green, D. W., R. H. Perry, and R. E. Babcock (1964), Longitudinal dispersion of thermal energy through porous media with a flowing fluid, *AIChE J.*, *10*(5), 645–651, doi:10.1002/aic.690100514.

Groffman, P. M., A. M. Dorsey, and P. M. Mayer (2005), N processing within geomorphic structures in urban streams, *J. N. Am. Benthol. Soc.*, *24*(3), 613–625, doi:10.1899/04-026.1.

Haggerty, R., and S. M. Gorelick (1995), Multiple-rate mass transfer for modeling diffusion and surface reactions in media with pore-scale heterogeneity, *Water Resour. Res.*, *31*(10), 2383–2400, doi:10.1029/95WR10583.

Haggerty, R., E. Martí, A. Argerich, D. von Schiller, and N. B. Grimm (2009), Resazurin as a "smart" tracer for quantifying metabolically active transient storage in stream ecosystems, *J. Geophys. Res.*, *114*, G03014, doi:10.1029/2008JG000942.

Harvey, J. W., and K. E. Bencala (1993), The effect of streambed topography on surface-subsurface water exchange in mountain catchments, *Water Resour. Res.*, *29*(1), 89–98, doi:10.1029/92WR01960.

Harvey, J. W., and C. C. Fuller (1998), Effect of enhanced manganese oxidation in the hyporheic zone on basin-scale geochemical mass balance, *Water Resour. Res.*, *34*(4), 623–636, doi:10.1029/97WR03606.

Harvey, J. W., and B. J. Wagner (2000), Quantifying hydrologic interactions between streams and their subsurface hyporheic zones, in *Streams and Ground Waters*, edited by J. A. Jones and P. J. Mulholland, pp. 3–44, Academic, San Diego, Calif.

Harvey, J. W., B. J. Wagner, and K. E. Bencala (1996), Evaluating the reliability of the stream tracer approach to characterize stream-subsurface water exchange, *Water Resour. Res.*, *32*(8), 2441–2451, doi:10.1029/96WR01268.

Hatch, C. E., A. T. Fisher, J. S. Revenaugh, J. Constantz, and C. Ruehl (2006), Quantifying surface water-groundwater interactions using time series analysis of streambed thermal records: Method development, *Water Resour. Res.*, *42*, W10410, doi:10.1029/2005WR004787.

Healy, R. W., and A. D. Ronan (1996), Documentation of computer program VS2DH for simulation of energy transport in variably saturated porous media–modification of the U.S. Geological Survey's computer program VS2DT, *U.S. Geol. Surv. Water-Resour. Invest. Rep. 96-4230*, U.S. Geol. Surv., Denver, Colo. [Available at http://pubs.er.usgs.gov/publication/wri964230]

Hedin, L. O., J. C. von Fischer, N. E. Ostrom, B. P. Kennedy, M. G. Brown, and G. P. Robertson (1998), Thermodynamic constraints on nitrogen transformations and other biogeochemical processes at soil-stream interfaces, *Ecology*, *79*(2), 684–703, doi:10.2307/176963.

Hester, E. T., and M. W. Doyle (2008), In-stream geomorphic structures as drivers of hyporheic exchange, *Water Resour. Res.*, *44*, W03417, doi:10.1029/2006WR005810.

Hester, E. T., M. W. Doyle, and G. C. Poole (2009), The influence of in-stream structures on summer water temperatures via induced hyporheic exchange, *Limnol. Oceanogr.*, *54*(1), 355–367, doi:10.4319/lo.2009.54.1.0355.

Hsieh, P. A., W. Wingle, and R. W. Healy (2000), VS2DI—A graphical software package for simulating fluid flow and solute or energy transport in variably saturated porous media, *U.S. Geol. Surv. Water-Resour. Invest. Rep. 99-4130*, U.S. Geol. Surv., Lakewood, Colo.

Ingebritsen, S., W. E. Sanford, and C. E. Neuzil (2006), *Groundwater in Geologic Processes*, 2nd ed., Cambridge Univ. Press, Cambridge, U. K.

Jones, J., and P. J. Mulholland (2000), *Streams and Ground Waters*, Academic, San Diego, Calif.

Kaushal, S. S., P. M. Groffman, P. M. Mayer, E. Striz, and A. J. Gold (2008), Effects of stream restoration on denitrification in an urbanizing watershed, *Ecol. Appl.*, *18*(3), 789–804, doi:10.1890/07-1159.1.

Kaushal, S. S., G. E. Likens, N. A. Jaworski, M. L. Pace, A. M. Sides, D. Seekell, K. T. Belt, D. H. Secor, and R. L. Wingate (2010), Rising stream and river temperatures in the United States, *Front. Ecol. Environ*, *8*, 461–466, doi:10.1890/090037.

Keery, J., A. Binley, N. Crook, and J. W. N. Smith (2007), Temporal and spatial variability of groundwater-surface water fluxes: Development and application of an analytical method using temperature time series, *J. Hydrol.*, *336*(1–2), 1–16, doi:10.1016/j.jhydrol.2006.12.003.

Kinouchi, T., H. Yagi, and M. Miyamoto (2007), Increase in stream temperature related to anthropogenic heat input from urban wastewater, *J. Hydrol.*, *335*(1–2), 78–88, doi:10.1016/j.jhydrol.2006.11.002.

Landon, M. K., D. L. Rus, and F. E. Harvey (2001), Comparison of instream methods for measuring hydraulic conductivity in sandy streambeds, *Ground Water*, *39*(6), 870–885, doi:10.1111/j.1745-6584.2001.tb02475.x.

Lapham, W. W. (1989), Use of temperature profiles beneath streams to determine rates of vertical groundwater flow and vertical hydraulic conductivity, *Water Supply Paper 2337*, U.S. Geol. Surv., Denver, Colo.

Lautz, L. K. (2010), Impacts of nonideal field conditions on vertical water velocity estimates from streambed temperature time series, *Water Resour. Res.*, *46*, W01509, doi:10.1029/2009WR007917.

Lautz, L. K., N. T. Kranes, and D. I. Siegel (2010), Heat tracing of heterogeneous hyporheic exchange adjacent to in-stream geomorphic features, *Hydrol. Processes*, *24*(21), 3074–3086, doi:10.1002/hyp.7723.

LeBlanc, R. T., R. D. Brown, and J. E. FitzGibbon (1997), Modeling the effects of land use change on the water temperature in unregulated urban streams, *J. Environ. Manage.*, *49*(4), 445–469, doi:10.1006/jema.1996.0106.

Metzger, T., S. Didierjean, and D. Maillet (2004), Optimal experimental estimation of thermal dispersion coefficients in porous media, *Int. J. Heat Mass Transfer*, *47*(14–16), 3341–3353, doi:10.1016/j.ijheatmasstransfer.2004.02.024.

Molina-Giraldo, N., P. Bayer, and P. Blum (2011), Evaluating the influence of thermal dispersion on temperature plumes from geothermal systems using analytical solutions, *Int. J. Therm. Sci.*, *50*(7), 1223–1231, doi:10.1016/j.ijthermalsci.2011.02.004.

Nelson, K. C., and M. A. Palmer (2007), Stream temperature surges under urbanization and climate change: Data, models, and responses, *J. Am. Water Resour. Assoc.*, *43*(2), 440–452, doi:10.1111/j.1752-1688.2007.00034.x.

O'Connor, B. L., and J. W. Harvey (2008), Scaling hyporheic exchange and its influence on biogeochemical reactions in aquatic ecosystems, *Water Resour. Res.*, *44*, W12423, doi:10.1029/2008WR007160.

Packman, A. I., and M. Salehin (2003), Relative roles of stream flow and sedimentary conditions in controlling hyporheic exchange, *Hydrobiologia*, *494*(1–3), 291–297, doi:10.1023/A:1025403424063.

Poole, G. C., and C. H. Berman (2001), An ecological perspective on in-stream temperature: Natural heat dynamics and mechanisms of human-caused thermal degradation, *Environ. Manage.*, *27*(6), 787–802, doi:10.1007/s002670010188.

Rau, G. C., M. S. Andersen, A. M. McCallum, and R. I. Acworth (2010), Analytical methods that use natural heat as a tracer to quantify surface water–groundwater exchange, evaluated using field temperature records, *Hydrogeol. J.*, *18*, 1093–1110.

Rau, G. C., M. S. Andersen, and R. I. Acworth (2012), Experimental investigation of the thermal dispersivity term and its significance in the heat transport equation for flow in sediments, *Water Resour. Res.*, *48*, W03511, doi:10.1029/2011WR011038.

Reynolds, W. D., D. E. Elrick, and E. G. Youngs (2002), Ring or Cylinder Infiltrometers, in *Methods of soil analysis: Part 4- Physical methods*, edited by J. H. Dane and G. C. Topp, pp. 818–844, Soil Society of America, Madison, Wis.

Richardson, C. P., and A. D. Parr (1988), Modified Fickian model for solute uptake by runoff, *J. Environ. Eng.*, *114*, 792–809, doi:10.1061/(ASCE)0733-9372(1988)114:4(792).

Shanafield, M., C. Hatch, and G. Pohll (2011), Uncertainty in thermal time series analysis estimates of streambed water flux, *Water Resour. Res.*, *47*, W03504, doi:10.1029/2010WR009574.

Silliman, S. E., J. Ramirez, and R. L. McCabe (1995), Quantifying downflow through creek sediments using temperature time series: One-dimensional solution incorporating measured surface temperature, *J. Hydrol.*, *167*(1–4), 99–119, doi:10.1016/0022-1694(94)02613-G.

Stallman, R. W. (1965), Steady one-dimensional fluid flow in a semi-infinite porous medium with sinusoidal surface temperature, *J. Geophys. Res.*, *70*(12), 2821–2827, doi:10.1029/JZ070i012p02821.

Stonedahl, S. H., J. W. Harvey, A. Wörman, M. Salehin, and A. I. Packman (2010), A multiscale model for integrating hyporheic exchange from ripples to meanders, *Water Resour. Res.*, *46*, W12539, doi:10.1029/2009WR008865.

Stonestrom, D. A., and J. Constantz (2003), Heat as a tool for studying the movement of ground water near streams, *Circular 1260*, U.S. Geol. Surv., Denver, Colo.

Storey, R. G., K. W. F. Howard, and D. D. Williams (2003), Factors controlling riffle-scale hyporheic exchange flows and their seasonal changes in a gaining stream: A three-dimensional groundwater flow model, *Water Resour. Res.*, *39*(2), 1034, doi:10.1029/2002WR001367.

Suzuki, S. (1960), Percolation measurements based on heat flow through soil with special reference to paddy fields, *J. Geophys. Res.*, *65*(9), 2883–2885, doi:10.1029/JZ065i009p02883.

Swanson, T. E., and M. B. Cardenas (2010), Diel heat transport within the hyporheic zone of a pool–riffle–pool sequence of a losing stream and

evaluation of models for fluid flux estimation using heat, *Limnol. Oceanogr.*, *55*(4), 1741–1754, doi:10.4319/lo.2010.55.4.1741.

Triska, F. J., V. C. Kennedy, R. J. Avanzino, G. W. Zellweger, and K. E. Bencala (1989), Retention and transport of nutrients in a third-order stream: Channel processes, *Ecology*, *70*(6), 1877–1892, doi:10.2307/1938119.

Valett, H. M., J. A. Morrice, C. N. Dahm, and M. E. Campana (1996), Parent lithology, surface-groundwater exchange, and nitrate retention in headwater streams, *Limnol. Oceanogr.*, *41*(2), 333–345, doi:10.4319/lo.1996.41.2.0333.

Wang, L., and P. Kanehl (2003), Influences of watershed urbanization and instream habitat on macroinvertebrates in cold water streams, *J. Am. Water Resour. Assoc.*, *39*(5), 1181–1196, doi:10.1111/j.1752-1688.2003.tb03701.x.

Winter, T. C., J. W. Harvey, O. L. Franke, and W. M. Alley (1998), Ground water and surface water: A single resource, *Circular 1139*, U.S. Geol. Surv., Denver, Colo.

Wondzell, S. M., and F. J. Swanson (1996), Seasonal and storm dynamics of the hyporheic zone of a 4th order mountain stream. I: Hydrologic processes, *J. N. Am. Benthol. Soc.*, *15*, 3–19, doi:10.2307/1467429.

Wroblicky, G. J., M. E. Campana, H. M. Valett, and C. N. Dahm (1998), Seasonal variation in surface-subsurface water exchange and lateral hyporheic area of two stream-aquifer systems, *Water Resour. Res.*, *34*(3), 317–328, doi:10.1029/97WR03285.